Journal of the Brazilian Society of Mechanical Sciences and Engineering (2021) 43:289
https://doi.org/10.1007/s40430-021-03005-5

TECHNICAL PAPER

A cooperative control framework of multiple unmanned aerial vehicles for dynamic oil spill cleanup

Samane Kaviri[1] · Ahmadreza Tahsiri[1] · Hamid D. Taghirad[2]

Received: 4 June 2020 / Accepted: 27 April 2021

Abstract

Oil spills within the marine environment are undesirable events caused by unavoidable economic activities of huge sea lane traffics. A tremendous effort has been made to tackle this problem within academia and industries; among them, the concept of autonomous vehicles for oil spill combating seems to provide a promising solution. This paper mainly proposes a cooperative deployment framework for unmanned aerial vehicles (UAVs) to perform oil spill cleanup missions with dispersant spraying. An appropriate oil density function is introduced by applying a Gaussian mixture model based on NOAA's advanced oil spill model (General NOAA Operational Modeling Environment). UAVs are then deployed to cover oil spills for spraying operations. This deployment problem is formulated as a coverage problem based on centroidal Voronoi tessellation to determine UAVs' optimal location. By transforming the coverage control problem into a target tracking one, an Integral Terminal Super Twisting Sliding Mode Control is provided to drive the UAVs to the optimal configuration. Furthermore, a novel spraying adjustment strategy is also designed to target the oil spills more accurately at the appropriate dosage. The effectiveness of the proposed framework is studied through a case study in the Abuzar oil field in the Persian Gulf. The results verify the performance of the cooperative oil spill cleanup framework in conjunction with advanced oil spill modeling. Moreover, it is concluded that the oil spill can be more effectively dispersed if the proposed spraying adjustment strategy is implemented.

Keywords Multi-agent systems · Unmanned aerial vehicle (UAV) · Oil spill cleanup · Distributed deployment · Centroidal Voronoi Tessellation (CVT)

List of symbols

φ	Gaussian mixture model (GMM)
A_j	Weight of the jth mixture component
μ_j	Mean of the jth mixture component
C_j	The covariance matrix of the jth mixture component
K	Number of mixture components
q	An arbitrary point in area $Q \in R^2$
$P = \{p_1, \ldots, p_N\}$	Location of N mobile agent/UAV
$V = \{V_1, \ldots, V_N\}$	Generalized Voronoi tessellation of Q
T_{V_i}	Centroid of the ith Voronoi cell
H	Coverage cost function
Ω	Overall residual rotor angular velocity
m	Mass of UAV
J_p	Propeller rotor inertia of UAV
u_l	Control input of each UAV, $l = 1, 2, 3, 4$
$(x, y, z, \phi, \theta, \psi)$	Generalized coordinate vector of each UAV (position and orientation)
g	Gravitational acceleration constant
$I_{x,y,z}$	Body inertia of UAV
F_d, τ_d	Disturbance vectors
$g\left(q, p_i\right)$	Spraying performance function
σ_s	Spread of spraying pattern

Technical editor: Celso Kazuyuki Morooka.

✉ Hamid D. Taghirad
Taghirad@kntu.ac.ir

Samane Kaviri
Samane_kaviri@ee.kntu.ac.ir

Ahmadreza Tahsiri
Tahsiri@eetd.kntu.ac.ir

[1] Department of Systems and Control, Faculty of Electrical Engineering, K. N. Toosi University of Technology, Tehran, Iran

[2] Department of Systems and Control, Faculty of Electrical Engineering, Advanced Robotics and Automated Systems, K. N. Toosi University of Technology, Tehran, Iran

Published online: 14 May 2021

β_i	Effectiveness of spraying operation for the *i*th UAV
L	Oil cleaning capability
M_{V_i}	The volume of pollution in the area of Voronoi cell V_i
Δ_i	Total spraying error of the i *t*h UAV
S	Sliding variable
$k_1,\ k_2,\ k_3,\ k_4$	Controller gains
$\xi = \left[\xi_1\ \xi_2\right]^T \in \mathbb{R}^2$	State vector in the second-order dynamic model of UAV
η	External disturbances in the second-order dynamic model

1 Introduction

Marine pollution caused by oil spills is a severe environmental issue that may potentially cause adverse effects on marine ecosystems. The Persian Gulf, which is considered as a hub for the global oil industry, is under permanent threat from oil spills due to oil exploitation, production and transportation. Statistics provided by the International Tanker Owners Pollution Federation (ITOPF) indicate that in spite of a downward trend in the total number of spill events, oil spills are continuously reported, and finding effective cleanup solutions is a stringent requirement [1]. Therefore, an effective oil spill response strategy is mandatory, even if only seldom used. Among all, the dispersant cleanup method as the most common non-mechanical one is useful in this issue [2]. The use of chemical dispersants is selected as a response option in circumstances that are likely to be effective based on the net environmental benefit analysis (NEBA). Dispersants may be applied as soon as possible at high speeds by aerial vehicles such as aircraft and helicopters [3]; however, these spraying techniques are not precise enough to focus only on the polluted area, and different elements should be taken into account for designing an effective response strategy. Proper treatment of oil spills with the dispersant necessitates a proper understanding of the dynamic behavior of the polluted area. Furthermore, from a practical point of view, the correct spraying strategy must be used to achieve the recommended treatment rate and prevent overdosing or underdosing [4, 5]. Therefore, an accurate and effective spraying strategy is required to track and cover the time-varying polluted area by supplying enough dispersant in a different part of the polluted area [6]. The essential component in applying dispersant is to benefit from unmanned vehicles as an emerging tool to assist humans in hazardous environments. The integration of these elements in one framework may significantly enhance the effectiveness of oil spill response actions.

One of the promising solutions for oil spill cleanup is the use of unmanned vehicles [7–9]. This idea dates back to the year 2010, when several novel methods such as Seaswarm [10] and Protei [11] were proposed. Recently, unmanned vehicles for oil spill cleaning are recommended in [12], which provides complete coverage of the polluted area with a single agent. The main drawback of this approach is that oil fate and movement issues are not addressed. As a strategy learned from universal collective behavior in nature and society, a team of unmanned vehicles can accomplish more complex tasks in a hazardous environment [13]. This concept has been proposed in [14], where a cooperative oil cleaning strategy for a team of surface autonomous vehicles is introduced. Nevertheless, the essential issue of the dynamic behavior of the oil spill is not modeled in [14]. Furthermore, the motion strategy of the agents is proposed as a simple back and forth motion that could result in further propagation of the contamination. Moreover, in [14] the multi-agent system is not able to optimally focus just on the polluted part of the mission area, which leads to excess energy consumption and longer mission time. Hence, efficient oil spill cleanup strategy for multi-agent systems remains limited in practical use.

The above researches are related to the coverage-based deployment problem where cooperation between agents is achieved using the mission area partitioning. Voronoi partitioning for coverage problem was introduced in [15], based on a gradient descent strategy in a static environment. In most Voronoi-based coverage problems, it is common to assume simple kinematic models for the robots, such as the single integrator [15] or the double and higher-order integrators [16]. However, in recent years more realistic dynamic models have received increasing attention by researchers for optimal deployment of dynamic vehicles, such as UAVs [17]. On the other hand, in a multi-agent coverage control problem, the critical feature of the environment is often modeled by a density function [18, 19]. In contrast to most existing problem formulations in the literature [17, 20], where the density function of the environment is static, oil spill coverage requires a framework that can work in a time-varying environment [9]. A distributed coverage control in the presence of a time-varying density function was proposed in [21], simplifying the problem by assuming that the initial position of the agents is at the Voronoi centroids. Unlike [21], in [22], a generalized coverage optimization method with a time-varying density function is proposed for single integrator agents that could be used only in a limited range of linear robotic systems.

In order to overcome these restrictions, this paper develops a distributed control framework of a group of UAVs for oil spill cleaning in such a way that dispersants concentrate in the more polluted area. In our problem formulation, the spatiotemporal density of the oil spills is modeled by a Gaussian mixture model (GMM), which utilizes a fast and advanced Lagrangian oil spill model (GNOME). Gaussian mixtures are flexible and powerful modeling tools for

environmental functions representation such as temperature, pollution or light [23]. Therefore, it is assumed that the oil concentration on the sea surface can be described as a mixture of Gaussian kernels. The output of the GNOME Lagrangian model is processed to calculate the parameters of this mixture model in different time steps. The main goal is to design a distributed deployment framework for mobile agents that can autonomously and actively track the oil spill density as a time-varying environment. The proposed framework is capable of deploying the agents in the appropriate locations; i.e., more agents are gathered in the area with higher oil concentration. Therefore, the desired configuration of the agents improves the encounter rate, and the dispersants hit the oil spill at the desired dosage.

The main contributions of this paper can be summarized in three aspects. First, a GMM-based method is adopted to represent the time-varying behavior of oil on the sea surface, where the location data of oil particles is derived by a fast but advanced Lagrangian oil spill model (NOAA's GNOME). Second, considering the nonlinear dynamics of most aerial robots, a modified optimal deployment strategy is proposed in the time-varying environment. Different from previous works [15, 21, 22], which use traditional Lloyd's CVT method, the optimal deployment problem is transformed into a target tracking problem, and a state-of-the-art controller strategy (super twisting sliding mode) is applied to track the desired configuration for UAVs. Finally, a spraying adjustment strategy is designed in order to reduce the over- or under-spraying of dispersants. It is able to autonomously adapt the UAV configuration to the oil spill distribution, which results in a displacement of the boundary between Voronoi cells of neighboring UAVs.

This article is organized as follows. Section 2.1 discusses how oil spill behavior is modeled as an objective for this paper. Based on the oil spill density function, the pollution confrontation problem is formulated as a distributed deployment problem in Sect. 2.2. Section 2.3 introduces a new spraying adjustment strategy to improve the dispersant encounter rate for oil spill confrontation. A cooperative control framework is then proposed using Voronoi tessellation, in which the spraying adjustment method is integrated into the computation of Voronoi regions. Numerical simulations in the Abuzar oil field case study are presented in Sect. 4 to verify the effectiveness of the proposed framework. Finally, Sect. 5 draws the conclusions of this work and some future research directions.

2 Preliminaries and methods

Figure 1 shows the main components of the proposed framework in this paper.

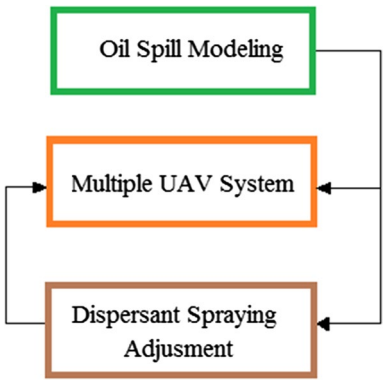

Fig. 1 Structure of the proposed framework for oil spill confrontation

In the upcoming subsections, the components of the proposed framework are presented and explained in more detail.

2.1 Oil spill modeling

In this section, the GNOME oil spill model is described briefly. Then, the details of GMM and parameter estimation of a GMM from the direct output of GNOME are explained. By this means, the mathematical relation of the oil intensity of each point in the polluted region caused by several oil spills is obtained.

2.1.1 NOAA's oil spill model

Oil spill simulation models can assist in directing cleanup efforts based on the predicted locations of the oil particles. Oil spill models can be mainly classified into two categories, numerical and analytical, which are used according to the intended application [24–26]. In this research, GNOME software is used for the modeling of oil spill scenarios. This software is a comprehensive numerical spill modeling package to predict the trajectory and spread of pollution from the initial state to its final state [27]. GNOME uses ocean current and local atmospheric conditions, as well as chemical and physical weathering processes [28]. The main GNOME output is a series of "Lagrangian elements (LEs)" that are released from a spill source and transported by wind, current and turbulent diffusion [29]. Each element is represented as a point in latitude and longitude format at each time step. The direct output of spill scenario simulating is information on the locations of LEs and their properties (mass, density, viscosity, etc.) for all time steps after the spillage [30].

Considering the stochastic nature of the ocean and local meteorological conditions, GNOME incorporates these uncertainties into the oil spill modeling. In addition to the best guess function for spill prediction, the minimum regret function is also considered in the prediction. By this means, GNOME may draw upon the modeling parameters set by a user and assume weather forecasts are accurate.

Furthermore, it may include a random component that will account for error or uncertainty in weather conditions [28]. The accuracy of output data of GNOME is directly related to the input condition of wind and current.

2.1.2 GMM-based oil distribution modeling

As a general rule, the outer edges of a typical oil slick are usually thinner than the inside of the slick [4]. Hence, the oil slick thickness may resemble a bivariate Gaussian distribution function of its coordinates x and y. One can assume that the pollution intensity at each point in a bounded mission area is a linear combination of continuous kernel functions with ideal weights [31, 32], especially at the early stage of spillage. Consequently, a Gaussian mixture model-based method can be considered and used to describe the oil spill concentration. In GMM-based modeling, it is assumed that the oil spill concentration on the sea surface is modeled by a mixture model, which is composed of K bivariate Gaussian density components. Parameter K is a positive integer that represents the number of oil slicks. Each component has a two-dimensional mean, μ_j, and 2-by-2 covariance matrix, C_j. The concentration density function over the mission area is given as follows:

$$\varphi(q,t)=\sum_{j=1}^{K}A_j(t)G\left(\mu_j(t),C_j(t)\right)=\sum_{j=1}^{K}A_j(t)\left[\exp\left(\left(q-\mu_j(t)\right)C_j(t)^{-1}\left(q-\mu_j(t)\right)^T\right)\right] \tag{1}$$

where φ is the Gaussian mixture model, and A_j, μ_j and C_j are the weight, mean and covariance matrix of the jth mixture component at each time step, respectively. The expectation–maximization (EM) algorithm is commonly used to fit GMM, while in this algorithm, an initial guess is set for the parameters, and then, it improves the estimates iteratively [33]. In this study, a modified EM algorithm proposed by McLachlan and Peel in [34] is employed to fit the GMMs.

A key task involved in the Gaussian mixture modeling for the environmental phenomenon is determining the best GMM fit by adjusting the number of components and the component covariance matrix structure. According to the purpose of this research and the complex behavior of oil spills, the number of components and the covariance matrix structure must be optimal in each step to achieve a more accurate model. For this purpose, the Bayesian information criterion (BIC) criterion has been used to determine the GMM model structure in this paper.

GMM is also considered as a soft clustering method that can accommodate clusters with different sizes and correlation structures, and hence, it is very suitable for our purpose. First, the algorithm is initiated by obtaining a set of candidate models for a range of values of K (from $K_{\min}$ to $K_{\max}$), which is assumed to contain the optimal K. Next, the BIC as one of the most widely used tools for statistical model selection [35], is exploited to determine the optimal number of the mixture components. To achieve more accurate GMMs, it is also better to consider the component covariance structure and examine the effect of the full or diagonal covariance matrix on BIC. Hence, The GMM with an optimal pair of K and an appropriate covariance structure has the lowest BIC.

It is necessary to convert the direct output of GNOME to an analytical function, such as a two-dimensional density function. Figure 2 illustrates the proposed procedure of the oil spill modeling to achieve a GMM. In the first part, the oil spill position data is clustered to determine the optimal number of (K) and the covariance matrix structure by minimizing the BIC criterion. By specifying the covariance matrices for each component as diagonal or full, the shape and orientation of the ellipsoids are determined. Geometrically, the covariance structure determines the shape of an ellipsoid drawn over a separated oil spill. The mean value, μ_j, for each oil slick represents the position of the highest level of oil concentration. In addition, the data of oil LEs for each oil slick is labeled according to the output of GMM clustering. The weights of components are calculated by converting the labeled output of GNOME to concentration, A_j, as shown in Fig. 2. To do so, first, the area of study is divided into several small rectangular polygons. Next, the concentration of oil in polygons near to the μ_j is calculated at each sample time. To compute the concentration of oil in a polygon at a specific time, the geographical locations of LEs are compared with the location of the polygon, and the total mass of particles within it is calculated and divided by its area. For the polygon near to the μ_j, the maximum concentration value in each data cluster is considered as A_j. Consequently, all the parameters of Eq. (1) are estimated for oil pollution at each sample time. It should be noted that, in this developed tool, the size of the rectangular polygons may be customized based on the spatial domain of the study.

Figure 3 represents the simulated oil spill distribution from two initial sources near 29.2 N 49.8 E. The spills leak on March 10, 2019, while 50 and 25 m^3 of medium crude oil are spilled on the water. This simulation assumes a northwesterly wind at the speed of 4 ms^{-1}. The results are presented in Fig. 3 at 4 h after the start of the spillage.

Figure 3a shows the GNOME simulation results. Figure 3b illustrates the processed results from the GMM-based clustering for the released oil spills, such that the number of oil spills and mean values are depicted. The black ×'s indicate the location of the mean value for each slick. Figure 3c represents the 3D visualization of the pollution density function, where

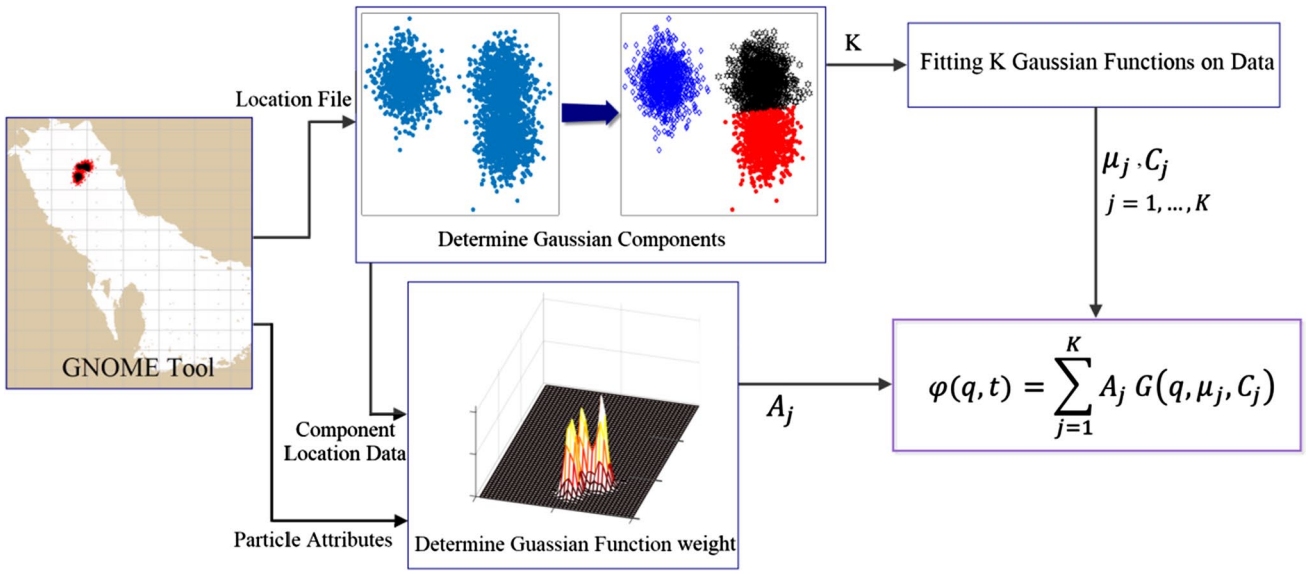

Fig. 2 Proposed oil spill distribution modeling based on a Lagrangian oil spill model

the brighter yellow color area illustrates the area with higher intensity of oil on the sea surface. It should be noted that the proposed method for oil spill modeling can also be used as a general spatial data analysis tool for density estimation and clustering of the data distributed over a mission space.

2.2 Autonomous multiple UAVs for oil spill confrontation

This paper introduces the deployment strategy of multiple UAVs with respect to the oil density function for cleaning marine oil pollution. In this section, we formulate our objectives into a formal problem. Consider a mission space as a convex area $Q \in R^2$, where $q \in \mathrm{Q}$ represents an arbitrary point in Q. In the mission area, $P = \{p_1, \ldots, p_N\}$ is the location of N mobile agent, i.e., p_i denotes the position of ith UAV in the mission area. Assume that each agent is equipped with localization devices and a downward spray. Suppose that the spray system directly interfaced with UAV's electronic systems to trigger spray release for oil cleaning tasks. We also assume that a UAV can communicate and exchange information with other UAVs. The state space of translational and rotational dynamics of each UAV can be obtained, respectively, as follows:

$$\begin{pmatrix} \ddot{x} \\ \ddot{y} \\ \ddot{z} \end{pmatrix} = -\begin{pmatrix} 0 \\ 0 \\ g \end{pmatrix} + \frac{1}{m}\begin{pmatrix} \cos\psi \sin\theta \cos\phi + \sin\psi \sin\phi \\ \sin\psi \sin\theta \cos\phi - \sin\psi \sin\phi \\ \cos\psi \cos\theta \end{pmatrix} u_1 + F_d$$

$$\begin{pmatrix} \ddot{\phi} \\ \ddot{\theta} \\ \ddot{\psi} \end{pmatrix} = f(\phi,\theta,\psi) + \mathrm{I}(\phi,\theta,\psi)\begin{pmatrix} u_2 \\ u_3 \\ u_4 \end{pmatrix} + \tau_d$$

$$f(\phi,\theta,\psi) = \begin{pmatrix} \dot{\theta}\dot{\psi}\left(\frac{I_y - I_z}{I_x}\right) - \frac{J_p}{I_x}\dot{\theta}\Omega \\ \dot{\phi}\dot{\psi}\left(\frac{I_z - I_x}{I_y}\right) - \frac{J_p}{I_y}\dot{\phi}\Omega \\ \dot{\phi}\dot{\theta}\left(\frac{I_x - I_y}{I_z}\right) \end{pmatrix}, \quad F_d = \begin{pmatrix} F_{dx} \\ F_{dy} \\ F_{dz} \end{pmatrix}, \quad \tau_d = \begin{pmatrix} \tau_{d\phi} \\ \tau_{d\theta} \\ \tau_{d\psi} \end{pmatrix}$$

$$\mathrm{I}(\phi,\theta,\psi) = \begin{pmatrix} \frac{1}{I_x} & 0 & 0 \\ 0 & \frac{1}{I_y} & 0 \\ 0 & 0 & \frac{1}{I_z} \end{pmatrix} \tag{2}$$

where $\Omega = -\omega_1 + \omega_2 - \omega_3 + \omega_4$ is the overall residual rotor angular velocity, m is the mass of UAV, J_p is the propeller rotor inertia,u_l control input for each $l = 1,2,3,4$ and $I_{x,y,z}$ are body inertia. F_d and τ_d are the vectors of the disturbances [36].

The agents have a spraying pattern, depending on the spray nozzle characteristics. The spraying performance is supposed to strictly decrease with respect to the distance between the position of the agent,p_i, and the point $q \in Q$ as represented by:

$$g(q,p_i) = g(q - p_i) = \beta_i(t) \exp\left(-\frac{(q_x - p_{xi})^2 + (q_y - p_{yi})^2}{\sigma_s^2}\right) \tag{3}$$

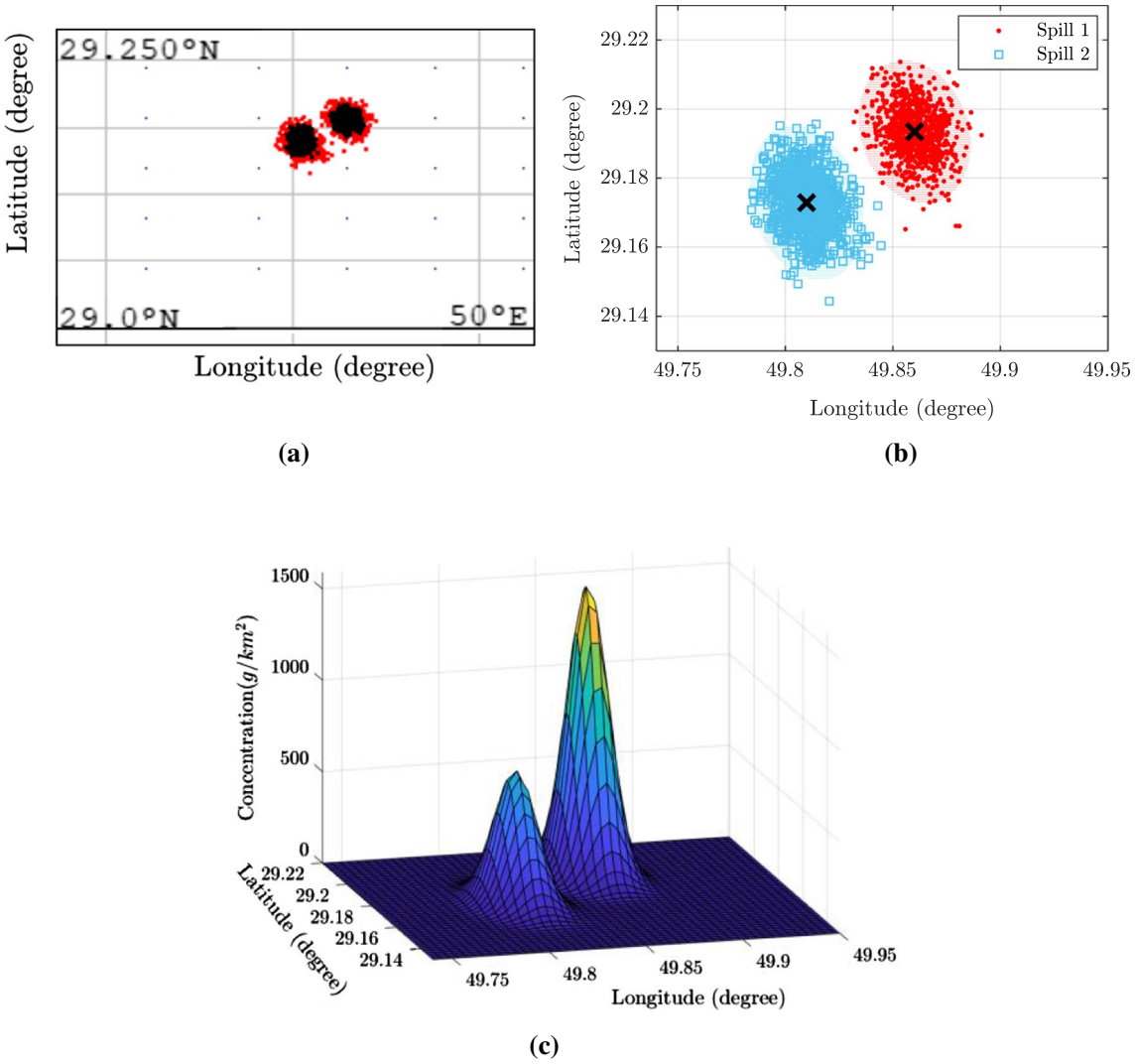

Fig. 3 GMM of oil distribution based on GNOME data. **a** Simulation result of GNOME shows oil spills LEs in the Persian Gulf, **b** The results from the GMM-based modeling, **c** 3D visualization of the oil concentration

where $r_i = \|q - p_i\|$, σ_s is the spread of spraying pattern and β_i is a positive adjustable value representing the effectiveness of spraying operation for the ith agent. Since the spraying effectiveness will attenuate to zero as $\|q - p_i\| \to \infty$, one can define the effective region of spraying by Ω_g (Fig. 4). The parameter β_i is defined to adjust the spraying effectiveness of each agent, which would be detailed in Sect. 2.3.

Due to the limited performance area of the agents, the mission area is first partitioned into subregions assigned to the agents using Voronoi partitioning. Assume that the movement of each robot is confined in Q and that $V = \{V_1, \ldots, V_N\}$ is a generalized Voronoi tessellation of Q such that$I(V_i) \cap I(V_j) = \emptyset$. $I(\cdot)$ denotes the interior space of each V_i and $\bigcup_{i=1}^{N} V_i = Q$. Therefore, it is supposed that each agent is only responsible for covering its domain V_i [22]. Based on Lloyd's algorithm, the region assigned to each agent called the Voronoi region is given by

$$V_i = \{q \in Q | g(q, p_i) \leq g(q, p_j), \forall j \neq i\} \tag{4}$$

In order to compute the Voronoi partition, it is assumed that through a fully connected communication network, each agent can share the position information with others in its neighboring Voronoi cells.

Our objective is to deploy a team of multiple UAVs to collaboratively cover a known oil spill in a specific region of the sea surface. Therefore, the coverage cost function in the mission space is defined as follows

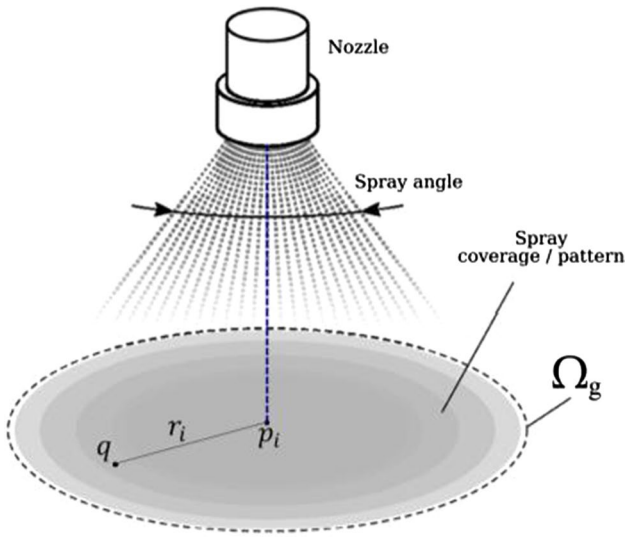

Fig. 4 Spraying pattern of each UAV

$$H(P,Q)=\sum_{i=1}^{N}H\left(p_i,V_i\right)=-\sum_{i=1}^{N}\int_{V_i}g\left(q,p_i\right)\varphi(q,t)dq \tag{5}$$

where V_i is the assigned region to ith UAV, $P=\left\{p_1,\ldots,p_N\right\}$ are the positions of the multiple UAVs, $g\left(q,p_i\right)$ means the spraying performance and $\varphi(q,t):Q\rightarrow R^{+}$ is the oil spill density function over the mission space at time t to obtain the adverse impact of the oil spill at the point $q\in Q$ in the mission area [15]. It is observed that the cost function is partly determined by the spraying performance in Eq. (3) and partly by the oil density function $\varphi(q,t)$. The density function adapts the objective function such that the UAVs will try to cover the field with more concentration on the polluted area.

We are seeking a distributed deployment strategy. That is, a collection of optimal trajectories to minimize the cost function $H(P,Q)$. Given a time-varying density function, which is strictly positive, mobile agents are deployed in a spatial configuration P^{*} such that the cost function H obtains a local minimum, i.e.,

$$P^{*}=\arg\min_{P}H(P,Q)\ \text{subject to (2)} \tag{6}$$

It should be noted that the minimum number of the required UAVs depends on three parameters, including the spilled oil volume, dispersant type and the loading capacity of each UAV. We assumed we had enough number of UAVs.

2.3 Spraying adjustment

Following a decision to apply dispersants, it is essential to consider the oil layer thickness as a relevant parameter to the dispersant dosage. By considering the oil areas with more thickness, it is possible to deploy the response tools to those areas specifically in order to increase their encounter rate significantly. In this paper, a Voronoi partitioning is proposed to deploy agents over a known environment by considering the oil density function. The main challenge in area partitioning for the cleanup mission is to allocate the appropriate volume of oil to the agents. Therefore, a new spraying adjustment method is defined for each agent, taking into account the spraying effectiveness in the spraying performance of the cost function.

The amount of dispersants that needs to be applied to a certain quantity of oil to achieve a desired level of dispersion mainly depends on the oil type, the ambient conditions and the dispersant type, which is determined by Dispersant to Oil Ratio (DOR) [37]. DOR is a beneficial measure to determine the amount of dispersant needed for the specific estimated oil volume. In this work, it is assumed that dispersants are divided equally between UAVs. Therefore, each UAV could clean a specific volume of oil represented by L. In order to make a meaningful criterion for the spraying quality of each agent, we rely on the local amounts of needed dispersant at each Voronoi cell. Thus, we can introduce M_i representing the volume of dispersant required for achieving ideal spraying (i.e., goal volume L) which can be calculated as follows:

$$M_i(t)=\mathrm{DOR}\left(\int_{V_i}\varphi(q,t)\mathrm{dq}\right)=\mathrm{DOR}M_{V_i}(t) \tag{7}$$

where $M_{V_i}(t)$ is the volume of pollution in the area of Voronoi cell V_i. When evaluating spraying precision, there are two aspects of inaccuracy to be considered: the errors produced in under-sprayed and over-sprayed regions. We calculate these errors as oil spill volume in these regions relative to the volume of oil for ideal spraying in the given region. The under-spray error is defined as

$$\Delta_i^{-}(t)=M_i(t)-L$$

where Δ_i^{-} represents the shortage of dispersants relative to the oil in its region. In contrast to the under-sprayed area, there are parts of the mission region where the applied dispersant would be excessive. They are considered by evaluating the over-spray error as:

$\Delta_i^{+}(t)=L-M_i(t)$.

Analogous to Δ_i^{-}, $\Delta_i^{+}$is the difference between the oil volume in the V_i and the goal volume. Although the errors Δ_i^{-} and Δ_i^{+} are rather intuitive, since they can be interpreted in terms of insufficiently and excessively applied dispersant, a distinct error relation is considered as:

$$\Delta_i(t)=L-M_i(t) \tag{8}$$

The practical meaning of the total error Δ_i is less intuitive. However, since it represents the overall misapplication of dispersant, the total error serves as a good measure of spraying accuracy. Obviously, Δ_i can be computed in a distributed manner within an individual Voronoi cell. However, $\varphi(q,t)$ is related to the whole mission space, which can only be obtained globally.

For the case of spraying adjustment, we choose an appropriately designed effectiveness parameter as:

$$\beta_i(t) = \beta_0 \exp\left(k_\beta \Delta_i(t)\right) \tag{9}$$

where $k_\beta > 0$ is adjustable parameters. The effectiveness parameter, $\beta_i(t)$, represents the spraying performance of the ith agent in its region as a function of spraying error Δ_i. The spraying adjustment affects the performance function $g(p_i, q)$ for each agent according to the misapplication of dispersant. By using the adjustment method (9), we investigate the effect of spraying adjustment on Voronoi partitioning in Proposition A.1 in Appendix. According to Eq. (21), when $\beta_i(t) > \beta_j(t)$, the distance between the point q and p_i would be more than that of p_j. It means that the actuation region for the agent with larger effectiveness intrudes on the other with a smaller one. Based on spraying adjustment in Eq. (9), the agent with a larger effectiveness value also has a larger spraying error Δ_i. In other words, the boundary of the region assigned to the agent with over-spraying error will move toward the Voronoi cell with an under-spraying error.

3 The proposed oil spill cleanup framework

This section presents a cooperative control framework for oil spill cleanup using a group of UAVs to cover the polluted area. According to the cost function (6), the proposed framework provides complete coverage in such a way that in thicker parts of the oil spill, more agents would be working. By coverage, we mean to deploy UAVs in an optimal location with respect to the oil spill density function. Then UAVs carry out a pollution cleanup operation by spraying the dispersant material to accelerate the oil dispersion. Consequently, the dispersant method would be utilized in an optimal manner. For this purpose, the optimal configuration of UAVs is first determined, and then, a distributed control strategy using Integral Terminal Super Twisting Sliding Mode Control (ITST-SMC) is designed for UAVs in order to track the time-varying optimal trajectories.

3.1 Optimal configuration

Based on the result in [22], the gradient of the cost function with respect to the ith agent position is given by

$$\frac{H(P,Q)}{\partial p_i} = \int_{V_i} \left(-2\frac{\partial g(q,p_i)}{\partial r_i^2} \right)(q - p_i)\varphi(q,t)\mathrm{d}q \tag{10}$$

By defining $\tilde{\varphi}\left(p_i,q,t\right) = -2\frac{\partial g(q,p_i)}{\partial {r_i}^2}\varphi(q,t)$, the mass and centroid of the ith Voronoi cell are defined as:

$$\tilde{M}_{V_i} = \int_{V_i} \tilde{\varphi}(p_i,q,t)\mathrm{d}q \tag{11}$$

$$T_{V_i} = \frac{1}{\tilde{M}_{V_i}} \int_{V_i} q\tilde{\varphi}(p_i,q,t)\mathrm{d}q \tag{12}$$

Hence, the gradient Eq. (10) can be written as

$$\frac{\partial H(P,Q)}{\partial p_i} = \tilde{M}_{V_i}\left(T_{V_i} - p_i\right) \tag{13}$$

If the generators of Voronoi tessellation $p_i, \ldots, p_N$ are also the centroids of their Voronoi cell, we have $\frac{\partial H(P,Q)}{\partial p_i} = 0$. Obviously, the local minimum points of the coverage cost (6) are the centroids of Voronoi cells, which results in

$$p_i^* = T_{V_i}, i = 1, \ldots, N \tag{14}$$

where p_i^* denotes the optimal position of the agent i. The agents' configuration is called a centroidal Voronoi tessellation (CVT) if they reach the centroid of their Voronoi partitions [15]. However, it is only a local minimum due to the nonlinear and non-convex property of $H(P,Q)$. We refer to [15, 38] for comprehensive treatments on locational optimization via Voronoi diagrams.

Whenever φ is time-variant, the CVT will be time-variant as well, and in this case, the CVT should be reached, and furthermore, the agents should track the time-varying CVT. As a result, the optimal deployment can be transformed into the desired point tracking problem. In the following section, the tracking problem is appropriately modeled, and by adopting ITST-SMC, a state-of-the-art nonlinear control strategy is proposed to handle this tracking problem.

3.2 ITST-SMC for optimal deployment

According to the optimal location of agents, as represented in Sect. 3.2, the tracking control strategy begins with defining the tracking error as the agent's distance from the centroid of its Voronoi cell as

$$e_i = p_i - T_{V_i} \tag{15}$$

Considering Eq. (15), the optimal deployment can be transformed into a time-varying trajectory tracking

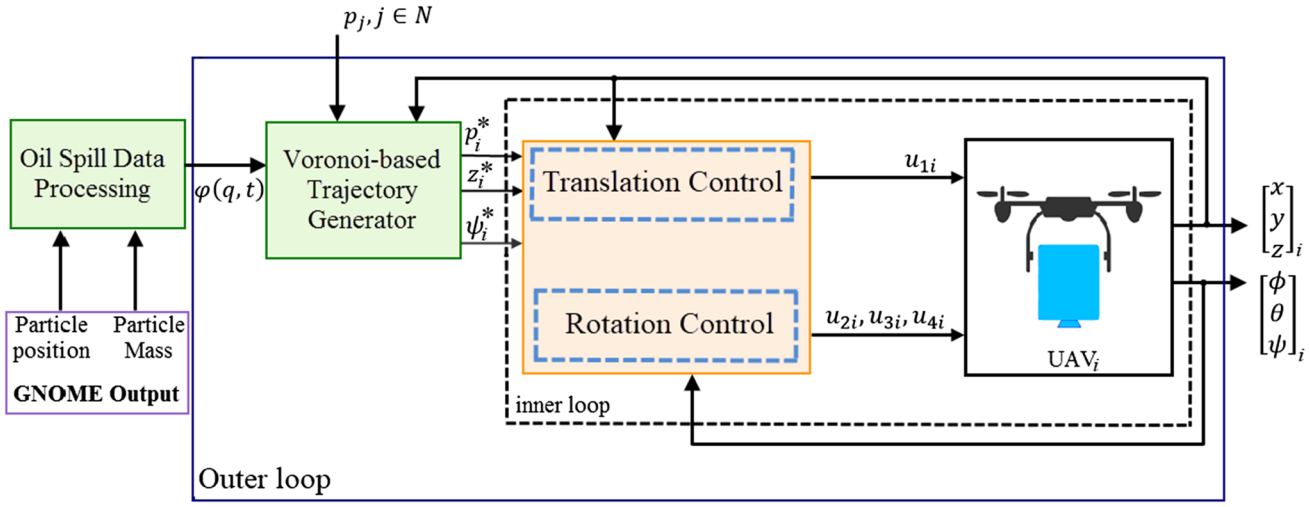

Fig. 5 Schematic of the proposed oil spill confrontation

problem, as represented in Fig. 5. As is seen in this figure, the control system of each UAV is composed of an outer loop generating the desired position command for the inner loop, which is focused just on the tracking control. It is necessary to maintain a safe distance to the water surface for UAVs represented by z^*. In the implementations of tracking control, the UAVs must reach this predefined altitude.

The following section proposes a solution to the tracking problem by incorporation of ITST-SMC. We consider the ITST-SMC as a baseline control law implemented individually on each UAV. The objective of the designed distributed control law is to converge the tracking error (15) toward zero for each agent. Based on [36], reformulate UAV dynamic model (2) as a second-order dynamic system defined by

$$\begin{aligned}\dot{\xi}_1(t) &= \xi_2(t)\\ \dot{\xi}_2(t) &= f(\xi(t)) + h(\xi(t))u(t) + \eta(t,\xi(t))\\ y(t) &= \xi_1(t)\end{aligned} \tag{16}$$

where $\xi = \begin{bmatrix}\xi_1 & \xi_2\end{bmatrix}^T \in \mathbb{R}^2$ represents the state vector,$y(t) \in \mathbb{R}$ is the system output, $u(t)$ is the input control, $f(\xi(t))$ and $h(\xi(t))$ are known functions extracted from Eq. (2). The term $\eta(t,\xi)$ includes external disturbances; for more details, please refer to work [36]. We assume that disturbance is bounded, and Lipschitz and $\dot{\eta}(t,\xi) < \hat{\eta}$.

Considering Eq. (16), the mathematical structure of ITST-SMC is presented for the case where all the state variables are available. Hereafter, the agent index will be omitted for simplicity in representation.

In the case of the second-order sliding mode control, for the sliding variable $S(\xi)$, the following condition should be verified

$$S(\xi) = \dot{S}(\xi) = 0 \tag{17}$$

Then, a nonlinear sliding surface with fractional dynamics is defined for system (16) as follows

$$S = e_2 + c_1 e_1 + c_2 \int_0^t e_1^{p/\lambda} d\tau \tag{18}$$

where $c_1, c_2 > 0$, p, λ are both positive odd integers satisfying the relation $p < \lambda$. The tracking errors are defined as $e_1 = \xi_1 - \xi_1^d$ and $e_2 = \xi_2 - \xi_2^d$ and the desired references are considered as ξ_1^d and ξ_2^d. The following theorem could analyze the finite time convergence of the sliding surface.

Proposition 1 *Consider control input* (19) *in the presence of external disturbance. The ITST-SMC* (19) *can guarantee the system trajectory to reach the sliding mode surface* (18) *in a finite time.*

$$u = h(\xi)^{-1}\left[-f(\xi) + \dot{\xi}_2^d - c_1\dot{e}_1 - c_2 e_1^{p/\lambda} - k_1|S|^{\frac{1}{2}}\mathrm{sgn}(S) - k_2 S - \int_0^t k_3\mathrm{sgn}(S)d\tau - k_4\int_0^t S d\tau\right] \tag{19}$$

According to [39, 40], *the proof of Proposition 1 is given in Appendix B.*

Note that the controller design process will use the variables $\dot{\xi}_2^d, \dot{\xi}_1^d$, *but to avoid numerical differentiation of* ξ_1^d, *the following second-order filter is used*

$$\ddot{\xi}_1^{\alpha} + 2\rho\omega\dot{\xi}_1^{\alpha} + \omega^2\left(\xi_1^{\alpha} - T_{V_i}\right) = 0 \tag{20}$$

where $\ddot{\xi}_1^{\alpha}$, $\dot{\xi}_1^{\alpha}$ *and* ξ_1^{α} *are the estimate values corresponding to* $\ddot{T}_{V_i}$, $\dot{T}_{V_i}$ *and* T_{V_i}.

It should be noted that a robust position and attitude control is designed by considering a time-scale separation between the translational dynamics and the orientation dynamics. This approach is based on the assumption that the closed-loop attitude dynamics converge faster than the closed-loop translational dynamics [41, 42]. *Desired references* $p_i^* = \left(x_i^*, y_i^*\right)$,$z_i^*$ *and* ψ_i^* *are generated by a trajectory generator in the outer loop of the proposed framework in Fig. 5, whereas references* φ_i^* *and* θ_i^* *are generated by using the dynamic equation of* $\ddot{x}_i$ *and* $\ddot{y}_i$ *in Eq. (2). We suggest the reader refer to* [36] *for more details.*

The control strategy for the UAVs is implemented in a distributed form, as depicted in Fig. 5. The Voronoi-based trajectory generator in the outer loop of Fig. 4. determines the new positions for the UAVs at each time step. To move to this new position, each UAV will use the ITST-SM control in the inner loop. Based on this framework, the closed-loop system converges to a centroidal Voronoi tessellation, and then, the dispersants would be sprayed on the oil spill. Therefore, we consider the UAV as a rigid body. Moreover, note that since each robot moves toward its Voronoi center, and no one could leave its Voronoi cell, there is no possibility of collision.

4 Results and discussion

4.1 Case study

The Persian Gulf is the largest offshore oil development area in the world. The frequency of oil spill events in this region is high because of extensive oil exploration and production activities [43]. Oil fields are hotspots with relatively high probabilities of oil spills in this area [27]. According to the result reported in [44], the Abuzar oil field is identified as a source that has a high level of oil spill risk. Therefore, this oil field (see Fig. 6a) is selected to examine the effectiveness of the proposed oil cleanup strategy. The most known weather phenomenon in the Persian Gulf is the Shamal, a northwesterly wind that prevails throughout the year [45]. Furthermore, there is an inverse estuarine circulation surface current pattern in the Persian Gulf, which is shown in Fig. 6b [44, 46].

Suppose that the crude oil is released near the Abuzar oil field (API = 26.9). It is assumed that the spill scenarios occur with a specific release amount, and the leakage stops before the inception of cleanup tasks. The defined scenarios are simulated by GNOME software. For these scenarios, each spill is considered by 1000 Lagrangian elements (LEs). According to the oil spill spreading and trajectory

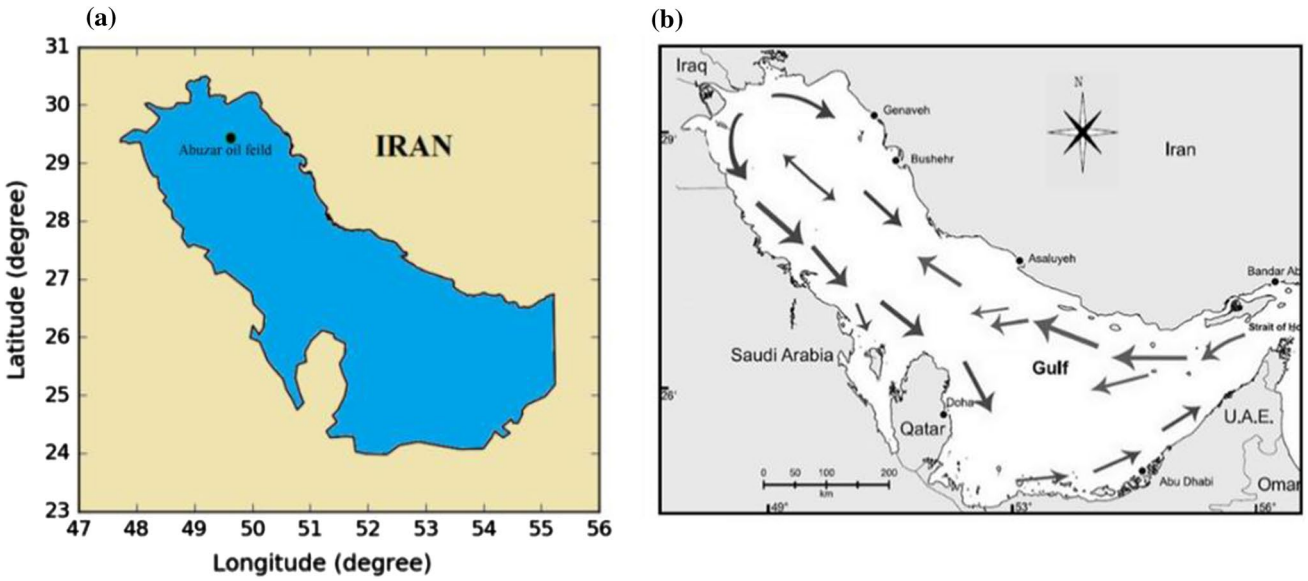

Fig. 6 Schematic diagram of the **a** Abuzar oil field, **b** general circulation of surface currents in the Persian Gulf [46]

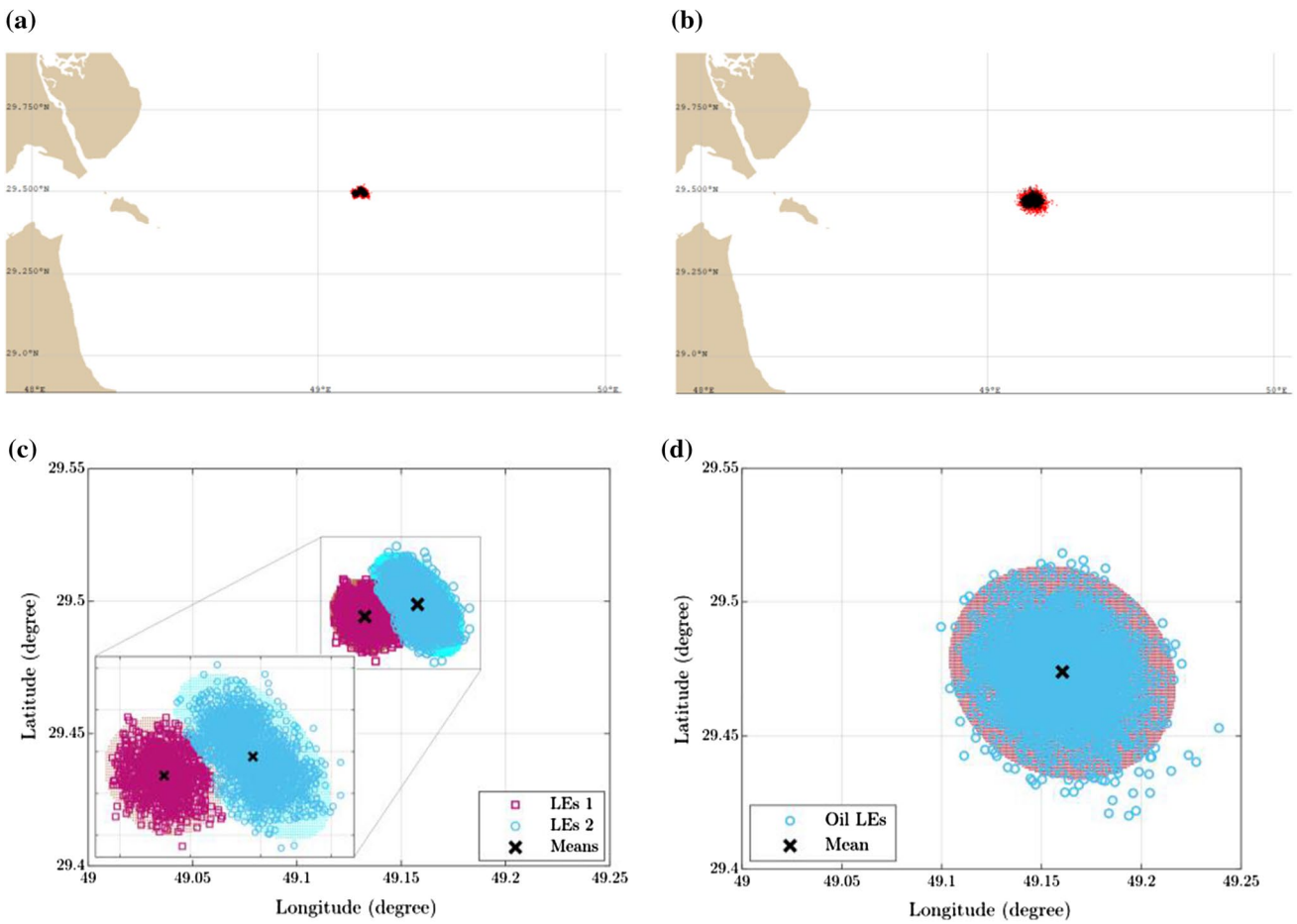

Fig. 7 Oil spill data distribution. **a** GNOME output at 12:00, **b** GNOME output at 20:00, **c** Estimated mean values of GMM at 12:00, **d** Estimated mean value of GMM at 20:00

in the defined scenario, the boundary of the mission area is determined.

4.2 Simulation results

The simulation results of the GMM-based oil spill modeling and cooperative oil spill confrontation in the Persian Gulf are presented in this section.

For the case of a northwesterly wind of 3 m/s, the result of simulations described in Sect. 2.1 for three oil spills is presented in Fig. 7 for one day. The oil pollution started with three initial oil spills near the latitude 29.5° N and longitude 49.1° E on March 19, 2019, 10:00, and in this event, 100 m^3 of crude oil is spilled on the water.

As indicated in Fig. 7, the released oil spreads and moves southward, and the oil slicks gradually merge into a single slick. The means of the Gaussian functions after 2 and 10 h after spillage are marked with black ×'s in Fig. 7c, d, respectively. As shown in these figures, the direct output of this Lagrangian spill model in different moments after the release is converted to GMM-based functions. The estimated parameters of the GMM components are presented in Table 1 at different time instants.

As shown in Table 1, the proposed algorithm in Sect. 2.1 determines the appropriate number of components for the oil spill distribution function as well as the appropriate GMM parameters. Considering the prevailing northwesterly wind (Shamal), the obtained graphical results in Fig. 7 are intuitively verified. Moreover, the validation of the GMM model was carried out by comparing numerical results in [27] with the proposed GMM solution in Fig. 8.

The comparison of models' results (concentration map and developed Lagrangian-based GMM model) show that the proposed model is a valid methodology for oil spill modeling with a similar result. Note that the GMM model is faster than the concentration map in terms of computation time.

Let us evaluate the proposed cooperative deployment framework with the processed data of GNOME. A rectangular area of 5 km × 7 km is considered such that X and Y axes are limited by the intervals (49.54° ,49.59°) N and (29.47° ,29.53°) E, respectively. We consider 20 UAVs with initial locations arbitrarily generated at the corner of the

Table 1 Estimated parameters of oil spill components at different time steps

Time	Number of oil spills (K)	Mean vector (μ_j)	Covariance matrix (C_j)
2019-03-19, 10:10	1	$[29.49\ \ 49.13]$	$10^{-4}\begin{bmatrix} 0.3582 & -0.0466 \\ -0.0466 & 0.2542 \end{bmatrix}$
	2	$[29.50\ \ 49.15]$	$10^{-4}\begin{bmatrix} 0.329 & -0.0083 \\ -0.0083 & 0.2111 \end{bmatrix}$
	3	$[29.49\ \ 49.16]$	$10^{-4}\begin{bmatrix} 0.4104 & -0.0538 \\ -0.0538 & 0.2602 \end{bmatrix}$
2019-03-19, 12:00	1	$[29.494\ \ 49.132]$	$10^{-4}\begin{bmatrix} 0.3606 & -0.0441 \\ -0.0441 & 0.2554 \end{bmatrix}$
	2	$[29.498\ \ 49.157]$	$10^{-4}\begin{bmatrix} 0.6274 & -0.2937 \\ -0.2937 & 0.05047 \end{bmatrix}$
2019-03-19, 20:00	1	$[29.473\ \ 49.160]$	$10^{-3}\begin{bmatrix} 0.4028 & -0.0380 \\ -0.0380 & 0.1998 \end{bmatrix}$

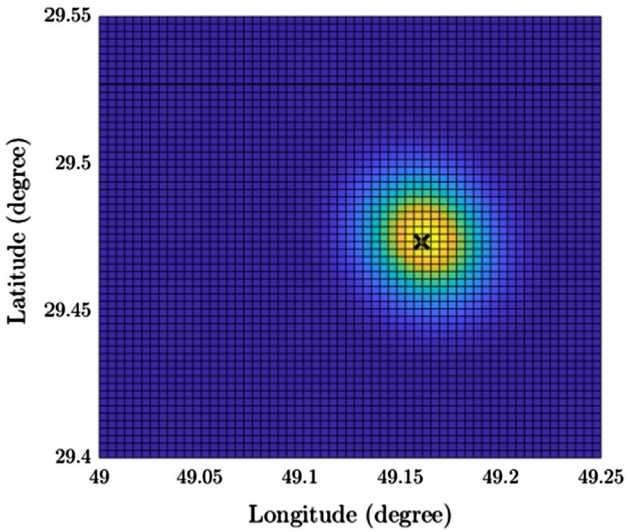

Fig. 8 Oil spill concentration map in [27] and mean value of GMM at 20:00

Table 2 UAV model parameters

Parameter	Value	Unit
m	2	kg
g	9.81	m/s^2
$I_x = I_y$	0.008	Ns^2/rad
I_z	0.02	Ns^2/rad
J_p	0.0001	Ns^2/rad

mission area with $z_i = 0$ from the rescue site or ship. Our simulation is conducted in MATLAB R2018b to validate this study for 3 h. In this study, the sea surface wind field is obtained from near-real-time measurements from ASCAT onboard MetOp (the Meteorological Operational platform) satellite. The ASCAT sea surface wind product is a 1-day composite product with a spatial resolution of 0.25° [47]. It may be seen that a variable northwesterly wind of 45 m/s prevailed in the study area during this period. In the spill scenario, two oil slick with 40 m^3 of crude oil are released near 29.50 N and 49.55 E on March 19, 2019, 10:00. It is assumed that the estimated parameters of GMM oil spill density are available for all of UAVs at each time step, and the GMM's parameters would be transmitted to the UAVs. The dynamic parameters of UAVs are shown in Table 2.

External disturbances are considered as $\eta_i = 0.1\sin(100\pi t)$, $i = 1,2,3$. The simulation parameters are defined as DOR $= 1:20, \sigma_s = 10, \lambda = 5, p = 3, L = 100, k_\beta = 2, \beta_0 = 2$. The controller parameters are chosen as: $k_{1\theta} = k_{1\psi} = k_{1\phi} = 11$, $k_{2\theta} = k_{2\psi} = k_{2\phi} = 6.5$, $k_{3\theta} = k_{3\psi} = k_{3\phi} = 4$, $k_{4\theta} = k_{4\psi} = k_{4\phi} = 2$, $k_{1x} = k_{3x} = k_{4x} = k_{4y} = k_{4z} = k_{3y} = 2, k_{2x} = k_{2z} = 3, k_{1y} = 2.1$, $k_{2y} = 4.2, k_{1z} = 5.2, k_{3z} = 2.75$.

The desired yaw angle is considered as $\psi_i^* = 0$, and the desired altitude is $z_i^* = 10$ m for all of the UAVs. Under motion control law (19) and in order to minimize the cost function (6), optimal deployment of UAVs at different time instants is shown in Fig. 9 from a top view (X–Y plane). Each UAV is indicated by a star shape, and the Voronoi cell of each UAV is denoted by white lines. The colorful background of Fig. 9 reflects the 2D representation of oil spill density function $\varphi(q,t)$ over the mission area, where the yellow parts represent the region with higher oil concentration.

Figure 9a depicts the initial configuration of UAVs and also presents the initial oil spill distribution. According to Fig. 9b, c, the UAVs followed the oil spill distribution changes. As the oil spill expanded, the UAVs simultaneously followed this expansion path. Finally, as shown in Fig. 9d, the UAVs covered the oil spill distribution very well. In order to cover the polluted area, from Fig. 9, we can see that each UAV attempts to move closer to the more polluted part of the

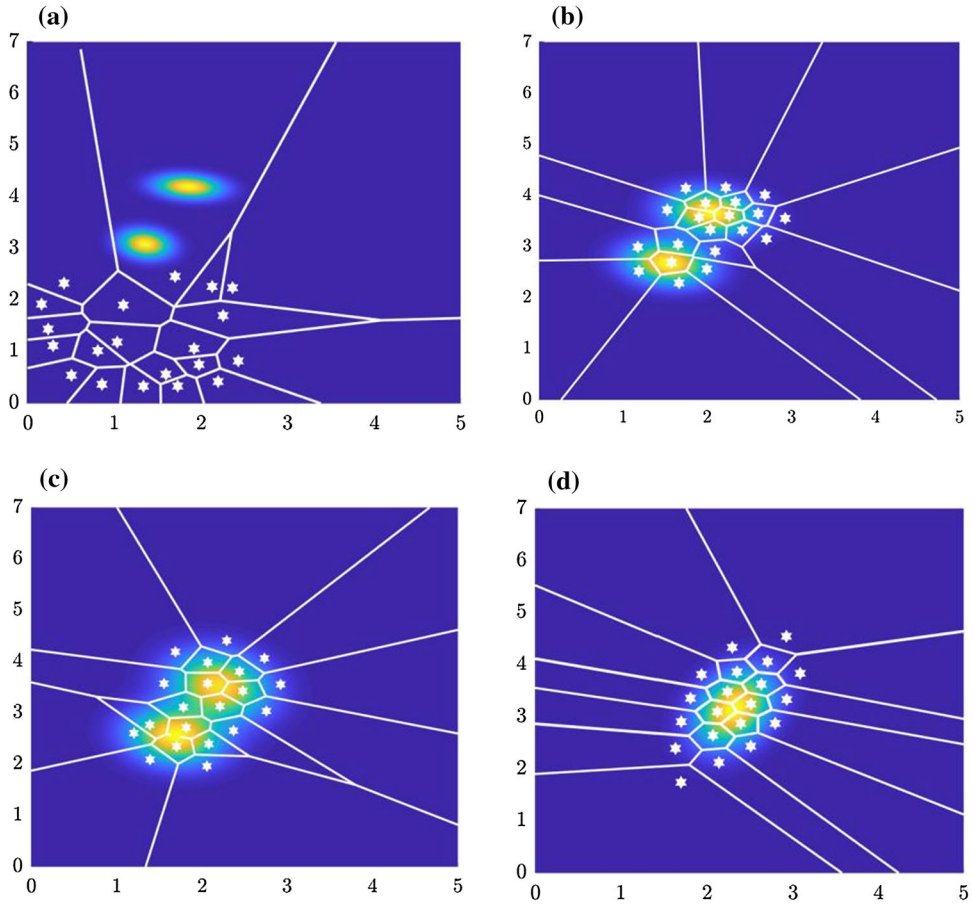

Fig. 9 Optimal deployment of mobile agent in different snapshots. **a** t = 11:00, **b** t = 11:30, **c** t = 12:30, **d** 13:00

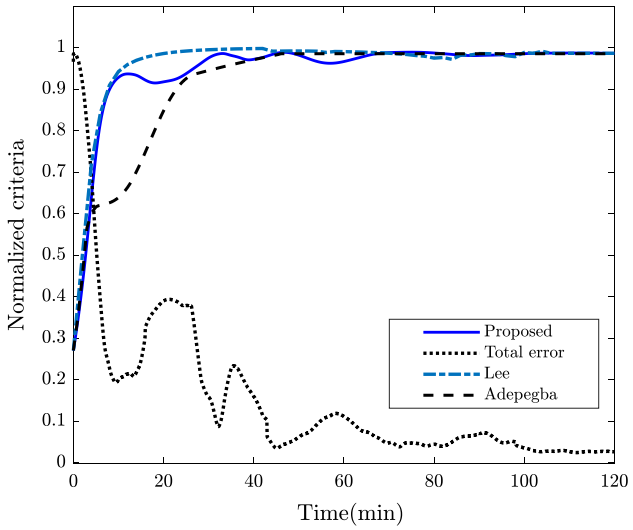

Fig. 10 Evolution of objective function and total tracking error

mission area due to the higher intensity of oil. Furthermore, the snapshots of the simulation results along time in Fig. 9 represent the effectiveness of the proposed controller (19). Accordingly, the desired tracking performance is achieved. The non-uniform configuration of UAVs in the mission area is triggered by the time-varying and non-uniform behavior of oil spill concentration on the sea surface.

As shown in Fig. 9, the UAVs will ultimately converge to their centroidal Voronoi tessellation. To verify the performance of the proposed control algorithm quantitatively, the time evolution of the normalized value of objective function $J = -\sum_{i=1}^{N} H(p_i, V_i)$ and total tracking error $E = \sum_{i=1}^{N} \|e_i\|$ are given in Fig. 10. In this simulation, we are trying to compare our proposed coverage framework in the time-varying environment with two of the most common gradient descent-based techniques in [21] for single integrator agents and [48] for double integrator agents.

It can be seen that the total tracking error reduces rapidly to a small value, while the objective function of the proposed framework, J, also increases noticeably, which indicates decreasing of the coverage cost function $H(P, Q)$. Figure 10 illustrates that the difference between the cost functions in the proposed framework and [21] is limited and converges to zero, which means that the configuration of agents reaches a near-optimal deployment. As expected, the coverage control strategy in [21] has the highest value of objective function compared to all the algorithms due to the first-order

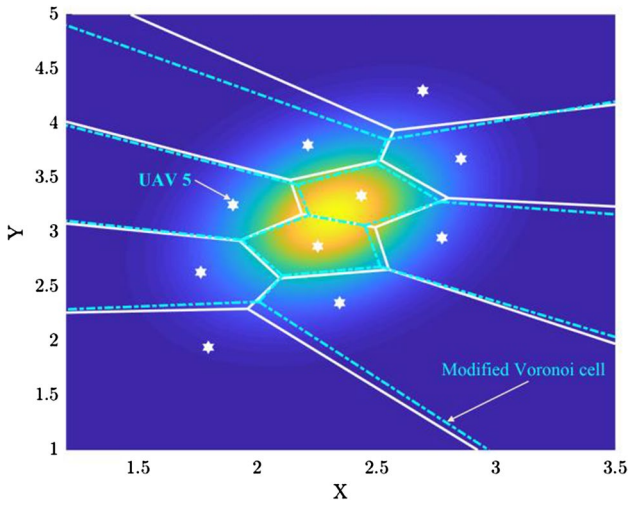

Fig. 11 Optimal deployment of UAVs with the spraying adjustment strategy. Dotted lines are the corresponding Voronoi tessellation and white solid lines are the Voronoi tessellation without spraying adjustment (colour figure online)

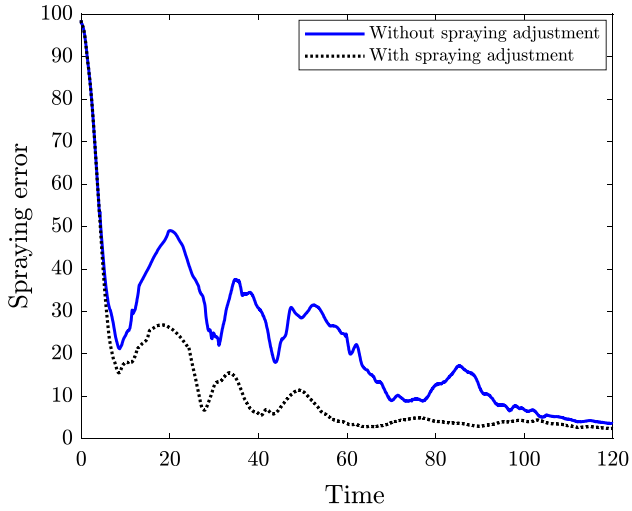

Fig. 12 Spraying error evolution for 5th UAV

kinematic of agents. By computing the objective function in [48] with our proposed control law, it is shown that our controller could find a better settling time to cover the area.

If the spraying adjustment strategy (8) proposed in this paper is implemented, the UAV spraying operation will be more balanced. Actually, the spraying adjustment method is a perturbation on the convergence of agents to their Voronoi centroids. Therefore, spraying adjusting action cannot be applied too frequently. Thus, a threshold is considered. The spraying adjustment strategy will be canceled when the spraying error of any agent is nearly the same with the goal volume or surpassing the maximum adjustable range. For better visualization, the evolution of optimal deployment for 10 UAVs using spraying adjustment strategy is depicted in Fig. 11. Since the spraying adjustment strategy is a perturbation on the convergence of the agents to the CVT, it is activated just for the range of $0.15L < \Delta_i < 0.6L$. As it is seen in this figure, the Voronoi cell with smaller spraying error encroaches upon other Voronoi cells, and the boundary of this Voronoi cell moves toward Voronoi cells with larger spraying errors.

From Fig. 11, the Voronoi cell with larger spraying deviation encroaches upon other Voronoi cells, since the agent with the larger value of effectiveness also has a larger spraying error Δ_i. Therefore, the boundary of this Voronoi cell moves toward Voronoi cells with the under-spraying error. For more clarifying the issue, Fig. 12 portrays the spraying error (8) for UAV 5, which is specified in Fig. 11.

Figure 12 clarifies that the Voronoi-based control strategy needs a longer time to reach a satisfactory spraying accuracy, but applying the proposed spraying adjustment can force the system to achieve the desired value with smaller error variation and better settling time.

This paper has developed a cooperative framework to use UAVs to cover a time-varying environment in an oil spill cleanup mission. However, it is also important to consider assessing the treatment operations after the start of dispersant spraying. Therefore, there are possible enhancements for the proposed oil spill cleanup framework, which may include a detailed experimental validation to assess the practical value of the proposed method or utilizing a heterogeneous group of unmanned agents (e.g., a combination of unmanned aerial and ground vehicles).

5 Conclusions

A cooperative framework based on a group of UAVs is proposed for offshore oil spill cleaning in a dynamic environment. In this framework, spill scenarios are first simulated by NOAA's GNOME, which is a fast Lagrangian trajectory model. Based on the results of GNOME, oil spill distribution is then identified using new GMM-based modeling. To mitigate the adverse environmental effects of oil spills, this research focuses on the distributed coordination of UAVs that can collaboratively track and cover a time-varying environment for dispersant spraying operations. A coverage cost function is defined to describe the performance of the response system and catch out the optimal locations for UAVs. On this basis, the coordination problem of UAVs is formulated as a tracking problem using Voronoi tessellation. Adopting sliding mode control method, a new distributed controller is provided to ensure that the UAVs approach the near-optimal configuration asymptotically. Moreover, it is

proposed that in order to improve the efficiency of the dispersant method, a spraying adjustment strategy could mitigate the misapplication of dispersants by considering the recommended dispersant to oil ratio.

In the simulated scenario in the Persian Gulf, the capability of the developed cooperative framework for oil spill confrontation is tested successfully. The simulation results are shown that the coverage cost function is further reduced when the spraying adjustment strategy is applied. Besides advantages, the most important constraint of the developed tool is that, in the existing version, cost and operational limitations of response methods have not been yet integrated into the model. Therefore, more research studies are required to extend it to real-world applications. We assumed that the entire oil spill data needed by UAVs are available for all of the agents. Although oil spill information can be obtained through remote sensing, this may not always be available due to communication constraints and cost. Thus, the autonomous agents are required to monitor the mission area while simultaneously covering the polluted parts. This issue is known as cooperative estimation and control for the unknown environment which is currently under research by the authors.

Appendix A

Proposition A.1 *Under-spraying adjustment strategy* (9), *the boundaries of Voronoi cells* V_i *with respect to spraying performance function* $g(q,p_i)$, $\forall i \in \{1,\dots,N\}$ *are straight line segments and the ith agent with larger spraying error* Δ_i *will intrude on its neighbor agents' Voronoi cells.*

Proof Consider an arbitrary point $q=(x,y)^T$ on the boundary of neighbor Voronoi cells V_i and V_j at a specific time. According to the geometric property of standard Voronoi partition, each point on the boundary between V_i and V_j satisfies $g(q,p_i)=g(q,p_j)$. Therefore, we have.

$$\beta_i(t)\exp\left(-\frac{q-p_i^2}{\sigma_s^2}\right)=\beta_j(t)\exp\left(-\frac{q-p_j^2}{\sigma_s^2}\right) \tag{21}$$

where $p_i=\left[p_{xi},p_{yi}\right]^T$ and $p_j=\left[p_{xj},p_{yj}\right]^T$ are agents' position. Then we can solve the point q from (21) as

$$y=\frac{(p_{xi}-p_{xj})}{(p_{yj}-p_{yi})}x+\frac{\sigma_s\left(\ln\left(\beta_i(t)/\beta_j(t)\right)\right)+\left(p_{xj}^2+p_{yj}^2\right)-\left(p_{xi}^2+p_{yi}^2\right)}{2\left((p_{yj}-p_{yi})\right)} \tag{22}$$

Hence, the boundary of two-agent is presented by

$$y=\mathcal{B}x+\mathcal{D} \tag{23}$$

where the parameters $\mathcal{B}$ and $\mathcal{D}$ are constants for a given position configuration $P(t)$. Since Eq. (23) holds true for any arbitrary point q on the boundary of Voronoi cells V_i and V_j; it can be concluded that all edges of Voronoi cells will remain straight line.

Appendix B

Proof of Proposition 1

The SMC stability analysis usually has two phases, namely a reaching phase and a sliding phase [39]. In reaching phase, the time derivative of the sliding surface, with the dynamic of the system (16), is given as

$$\dot{S}=f(\xi(t))+h(\xi(t))u(t)+\eta(t,\xi(t))-\dot{\xi}_2^d+c_1\dot{e}_1+c_2e_1^{p/\lambda} \tag{24}$$

Substituting the ITST-SMC (19) in (24), we obtain

$$\dot{S}=-k_1|S|^{\frac{1}{2}}\mathrm{sgn}(S)-k_2S-\int_0^t k_3\mathrm{sgn}(S)d\tau-k_4\int_0^t Sd\tau+\eta(t,\xi(t)) \tag{25}$$

Consider the new variables ρ_1 and ρ_2 as

$$\rho_1=S,\quad \rho_2=-\int_0^t k_3\mathrm{sgn}(S)d\tau-k_4\int_0^t Sd\tau+\eta(t,\xi(t)) \tag{26}$$

Thus, the sliding surface dynamic could be rewritten as follows

$$\begin{aligned}\dot{\rho}_1&=-k_1\left|\rho_1\right|^{\frac{1}{2}}\mathrm{sgn}\left(\rho_1\right)-k_2\rho_1+\rho_2\\ \dot{\rho}_2&=-k_3\mathrm{sgn}\left(\rho_1\right)-k_4\rho_1+\dot{\eta}\end{aligned} \tag{27}$$

Equation (27) is equivalent to those for a second-order sliding mode with a linear growing perturbations system as given in [40]. The details of convergence proofs for (27) are presented in [40]. Hence, by appropriately selecting the gains k_1, k_2, k_3, k_4, the finite time convergence to the sliding surface $S=0$ is ensured. Suppose that for the system (16), the derivative of the disturbance is globally bounded by $|\dot{\eta}|<\eta_1+\eta_2|\rho_1|$ with $\eta_1>0$ and $\eta_2>0$, assuming that the gains k_1, k_2, k_3, k_4 are selected according to

$$
\begin{aligned}
&k_1 > \sqrt{\eta_1}\\
&k_2 > \frac{1}{2}\sqrt{8\eta_2}\\
&k_3 > \eta_1\\
&k_4 > \frac{k_1\left[\frac{1}{2}k_1^3(2k_2-\eta_2)+\left(\frac{5}{2}k_2^2+\eta_2\right)\rangle\right]}{2} = k_1\left[\left(\frac{1}{4}k_1^2-\eta_1\right)+\frac{1}{2}k_1\left(2k_3+\frac{1}{2}k_1^2\right)\right]
\end{aligned}
\tag{28}
$$

Then, the ITST-SMC (19) yields finite time convergence of the sliding surface [40]. Meanwhile, it is obtained that $\dot{S}(\xi) = 0$. Once the state vector reaches the sliding surface (18), the following result establishes that the tracking error will asymptotically converge to zero. According to Eq. (17), the time derivative of the sliding surface is obtained as

$$\dot{e}_2 + c_1\dot{e}_1 + c_2 e_1^{p/\lambda} = 0 \tag{29}$$

or

$$\dot{e}_2 = -c_2 e_1^{p/\lambda} - c_1\dot{e}_1 \tag{30}$$

Choose the Lyapunov function candidate as

$$V = \frac{1}{2}e_2^2 + \frac{c_2 p}{\lambda + p}e_1^{(p/\lambda)+1} \tag{31}$$

Differentiate V with respect to time and apply (30) on the sliding surface, reach to:

$$
\begin{aligned}
&\dot{V} = e_2\dot{e}_2 + c_2\dot{e}_1 e_1^{p/\lambda} = e_2\left(-c_2 e_1^{p/\lambda} - c_1\dot{e}_1\right) + c_2\dot{e}_1 e_1^{p/\lambda}\\
&= e_2\left(-c_2 e_1^{p/\lambda} - c_1 e_2\right) + c_2 e_2 e_1^{p/\lambda} = -c_1 e_2^2\\
&\dot{V} \le 0
\end{aligned}
\tag{32}
$$

Therefore, $\dot{V}$ is negative definite, and consequently, all the states are uniformly bounded and tracking error will asymptotically converge to zero [39]. Thus, the ITST-SMC guarantees that tracking errors converge to the sliding surface S in a finite time and remain on it. Here, the goal is that the positions $p_i, \forall i \in \{1, \ldots, N\}$ asymptotically converge to their optimal trajectories T_{V_i}. By using the proposed result for the convergence of tracking error,e_1, we can conclude that p_i converge to the T_{V_i}.

Acknowledgements The authors sincerely acknowledge the NOAA's Office of Response and Restoration for sharing the GNOME code and their experience in oil spill modeling.

Funding The authors received no financial support for the research, authorship and publication of this article.

Declaration

Conflicts of interest The authors declare that they have no conflicts of interest.

References

1. ITOPF (2018) Statistics – ITOPF http://www.itopf.com/knowledge-resources/data-statistics/statistics/. Accessed 20 March 2020
2. National Research Council (2005) Understanding oil spl dispersants: efficacy and effects. National academy of science, Washington
3. Schrope M (2013) Researchers debate oil-spill remedy. Nature 493:461
4. Fingas M (2015) Handbook of oil spill science and technology. Wiley online library, Hoboken, New Jersey
5. EMSA (2009) Manual on the applicability of oil spill dispersants-version 2. www.emsa.europa.eu › opr-documents. Accessed 1 April 2020
6. Fingas M (2012) The basics of oil spill cleanup. CRC Press, New York
7. Hall S (2018) The Application of unmanned aerial systems UAS's to improve emergency oil spill response. In: Paper presented at the SPE international conference and exhibition on health, safety, security, environment, andsocial responsibility, Abu Dhabi, UAE, April 2018. https://doi.org/10.2118/190586-MS
8. Jokar H, Vatankhah R (2020) Adaptive fuzzy global fast terminal sliding mode control of an over-actuated flying robot. J Braz Soc Mech Sci Eng 42(4):1–18
9. Kaviri S Tahsiri A Taghirad HD (2019) Coverage control of multi-robot system for dynamic cleaning of oil spills. In: 2019 7th international conference on robotics and mechatronics (ICRoM). IEEE, pp. 17–22
10. MIT (2010) MIT researchers unveil autonomous oil-absorbing robot. MIT Media Relations. http://senseable.mit.edu/seaswarm/ss_prototype.html. Accessed 5 April 2020
11. Protei (2010) Protei: open source sailing drone. https:// www.kickstarter.com/projects/ cesarminoru/ protei-open-hardware-oil-spill-cleaning-sailing-ro. Accessed 10 April 2020
12. Jin X, Ray A (2014) Navigation of autonomous vehicles for oil spill cleaning in dynamic and uncertain environments. Int J Control 87:787–801
13. Viana ÍB, dos Santos DA, Góes LCS (2018) Formation control of multirotor aerial vehicles using decentralized MPC. J Braz Soc Mech Sci Eng 40(6):306
14. Song J, Gupta S, Hare J (2014) Game-theoretic cooperative coverage using autonomous vehicles. In: Proceedings of the MTS/IEEE OCEANS'14, 14–19 Sept 2014, St. John's, NL, Canada, pp 1–6. https://doi.org/10.1109/OCEANS.2014.7003082
15. Cortes J, Martinez S, Karatas T, Bullo F (2004) Coverage control for mobile sensing networks. IEEE Trans Robot Autom 20:243–255

16. Franceschelli M Egerstedt M Giua A Mahulea C (2009) Constrained invariant motions for networked multi-agent systems. In: 2009 american control conference, IEEE, pp. 5749–5754
17. Yan M, Guo Y, Zuo L, Yang P (2018) Information-based optimal deployment for a group of dynamic unicycles. Int J Control Autom Syst 16:1824–1832
18. Luo K, Guan ZH, Cai CX, Zhang DX, Lai Q, Xiao JW (2019) Coordination of nonholonomic mobile robots for diffusive threat defense. J Franklin Inst 356:4690–4715
19. Mavrommati A, Tzorakoleftherakis E, Abraham I, Murphey TD (2017) Real-time area coverage and target localization using receding-horizon ergodic exploration. IEEE Trans Rob 34:62–80
20. Mohseni F, Doustmohammadi A, Menhaj MB (2014) Distributed receding horizon coverage control for multiple mobile robots. IEEE Syst J 10:198–207
21. Lee SG, Diaz-Mercado Y, Egerstedt M (2015) Multirobot control using time-varying density functions. IEEE Trans Rob 31:489–493
22. Miah S, Panah AY, Fallah MMH, Spinello D (2017) Generalized non-autonomous metric optimization for area coverage problems with mobile autonomous agents. Automatica 80:295–299
23. Safarinejadian B, Hasanpour K (2014) Distributed data clustering using mobile agents and EM algorithm. IEEE Syst J 10:281–289
24. Berry A, Dabrowski T, Lyons K (2012) The oil spill model OILTRANS and its application to the Celtic Sea. Mar Pollut Bull 64(11):2489–2501
25. Nagheeby M, Kolahdoozan M (2010) Numerical modeling of two-phase fluid flow and oil slick transport in estuarine water. Int J Environ Sci Technol 7(4):771–784
26. Aghajanloo K, Pirooz MD, Namin MM (2013) Numerical simulation of oil spill behavior in the Persian Gulf. Int J Environ Res 7(1):81–96
27. Amir-Heidari P, Raie M (2019) Response planning for accidental oil spills in Persian Gulf: a decision support system (DSS) based on consequence modeling. Mar Pollut Bull 140:116–128
28. Grubesic TH, Wei R, Nelson J (2017) Optimizing oil spill cleanup efforts: A tactical approach and evaluation framework. Mar Pollut Bull 125:318–329
29. Zelenke B O'Connor C Barker CH Beegle-Krause C Eclipse L (2012) General NOAA operational modeling environment (GNOME). Technical documentation. https://response.restoration.noaa.gov. Accessed 29 April 2020
30. NOAA (2002) General NOAA Oil Modeling Environment (GNOME) User's Manual. https://response.restoration.noaa.gov/oil-and-chemical-spills/oil-spills/response-tools/gnome-suite-oil-spill-modeling.html. Accessed 29 April 2020
31. La HM, Sheng W (2013) Distributed sensor fusion for scalar field mapping using mobile sensor networks. IEEE Trans Cybern 43(2):766–778
32. Zuo L, Shi Y, Yan W (2017) Dynamic coverage control in a time-varying environment using Bayesian prediction. IEEE Trans Cybern 49(1):354–362
33. Tan PN, Steinbach M, Kumar V (2006) Introduction to data mining. Pearson addison wesley, Boston
34. McLachlan GJ, Peel D (2004) Finite mixture models. John wiley & sons, Hoboken
35. Hsu D (2015) Comparison of integrated clustering methods for accurate and stable prediction of building energy consumption data. Appl Energy 160:153–163
36. Modirrousta A, Khodabandeh M (2015) A novel nonlinear hybrid controller design for an uncertain quadrotor with disturbances. Aerosp Sci Technol 45:294–308
37. Grote M et al (2018) The potential for dispersant use as a maritime oil spill response measure in German waters. Mar Pollut Bull 129:623–632
38. Cortés J, Martinez S, Karatas T, Bullo F (2002) Coverage control for mobile sensing networks: Variations on a theme. In: Proceedings of the 10th Mediterranean conference on control and automation - MED2002, July 9–12, Lisbon, Portugal Lisbon, Portugal, pp 9–13
39. Wang Z, Li Q, Li S (2019) Adaptive integral-type terminal sliding mode fault tolerant control for spacecraft attitude tracking. IEEE Access 7:35195–35207
40. Moreno JA, Osorio M A (2008) Lyapunov approach to second-order sliding mode controllers and observers. In: 2008 47th IEEE conference on decision and control. IEEE, pp. 2856–2861
41. Bertrand S, Guénard N, Hamel T, Piet-Lahanier H, Eck L (2011) A hierarchical controller for miniature VTOL UAVs: design and stability analysis using singular perturbation theory. Control Eng Pract 19(10):1099–1108
42. Liu H, Bai Y, Lu G, Shi Z, Zhong Y (2014) Robust tracking control of a quadrotor helicopter. J Intell Rob Syst 75(3):595–608
43. Marine Traffic (2018) global ship tracking intelligence. https://www.marinetraffic.com/en/ais/home/centerx:54.7/centery:27.8/zoom:4. Accessed 1 April 2020
44. Amir-Heidari P, Raie M (2018) Probabilistic risk assessment of oil spill from offshore oil wells in Persian Gulf. Mar Pollut Bull 136:291–299
45. Pous S, Lazure P, Carton X (2015) A model of the general circulation in the Persian Gulf and in the Strait of Hormuz: intraseasonal to interannual variability continental. Shelf Res 94:55–70
46. Reynolds RM (1993) Physical oceanography of the Persian Gulf, Strait of Hormuz, and the Gulf of Oman—results from the Mt. Mitchell Exped Mar Pollut Bull 27:35–59
47. Xu Q, Li X, Wei Y, Tang Z, Cheng Y, Pichel WG (2013) Satellite observations and modeling of oil spill trajectories in the Bohai Sea. Mar Pollut Bull 71:107–116
48. Adepegba AA, Miah S, Spinell, D (2016, March) Multi-agent area coverage control using reinforcement learning. In: FLAIRS Conference, pp. 368–373.